International Journal of Mass Spectrometry 280 (2009) 179–183

Contents lists available at ScienceDirect

International Journal of Mass Spectrometry

journal homepage: www.elsevier.com/locate/ijms

Stark mixing by ion-Rydberg atom (molecule) collisions

G.S. Balaraman, M.R. Flannery*

School of Physics, Georgia Institute of Technology, Atlanta, GA 30332, USA

ARTICLE INFO

Article history:
Received 12 July 2008
Received in revised form 21 August 2008
Accepted 23 August 2008
Available online 2 September 2008

PACS:
34.50.Pi
34.60.+z
34.10.+x

Keywords:
Stark mixing
Ion–molecule collision
Angular momentum change

ABSTRACT

Classical molecular dynamics simulations are performed to cover Stark mixing transitions ($n\ell \to n\ell'$) in Rydberg atoms by collision with slow ions. Accuracy is tested by comparison with the exact analytical classical probabilities $P^{(n)}_{\ell'\ell}$ previously obtained when the ion–atom potential is taken as the long-range ion–dipole interaction. The results are provided not only for the ion–dipole interaction but also for the full electrostatic interaction. It is shown, by comparison, that the ion–dipole potential alone provides reliable probabilities. The method is highly accurate and is very amenable to ready inclusion of other processes competing with Stark mixing.

1. Introduction

The ion-Rydberg atom/molecule collisional process

$$A^{Z+} + Ry(n, \ell) \to A^{Z+} + Ry(n, \ell') \tag{1}$$

is called collisional Stark mixing [1–5] since the ℓ-changing transitions $\ell \to \ell'$ occur within the same energy shell n of the Rydberg species and are induced by the time-dependent electric field generated by the passing ion A^{Z+}. A Ryberg molecule with its orbiting electron in state (n, ℓ) can be considered [6] as a Rydberg atom $Ry(n, \ell)$, particularly for the higher ℓ when there is little penetration with the molecular ionic core. The ion–atom (molecule) electrostatic interaction

$$V(\mathbf{r}, \mathbf{R}) = \frac{Ze^2}{R} - \frac{Ze^2}{|\mathbf{R} - \mathbf{r}|} \tag{2}$$

between the ion, at position $\mathbf{R}$ from the atom whose Rydberg electron is at $\mathbf{r}$, has the long-range ($R \gg r$) multipole expansion

$$V(\mathbf{r}, \mathbf{R}) \to -\left(\frac{Ze^2}{R^2}\right) r\cos\theta - \left(\frac{Ze^2}{2R^3}\right)(3\cos^2\theta - 1) + \ldots \tag{3}$$

where θ is the angle between $\mathbf{R}$ and $\mathbf{r}$. At very large ion–atom separations $R \gg n^2 a_0$, the first term in the RHS of Eq. (3)– the ion–dipole interaction – dominates and induces $\ell \to \ell \pm 1$ transitions at a given time during the collision. When the collision is fast, then there is time only for the dipole $\ell \rightleftharpoons \ell \pm 1$ transitions to occur. For collisions at ultracold energies, there is abundant time during the collision for transitions to occur sequentially, as in the ladder $\ell \rightleftharpoons (\ell+1, \ell-1) \rightleftharpoons (\ell+2, \ell, \ell-2) \rightleftharpoons (\ell+3, \ell+1, \ell-1, \ell-3)$ and so on, the range of ℓ' depending on the duration of collision. In this sequential $\ell \rightleftharpoons \ell \pm 1$ tree-like way, a distribution of final ℓ' states can occur over a wide range of ℓ' values and this range widens as the collision energy is reduced so that all ℓ' states within the n-manifold can be eventually populated. This sequence depends on the accuracy/quality of the wave-function taken for the time-dependent perturbed Rydberg atom. For example, when unperturbed Rydberg wavefunctions are used, as in the Born approximation, then the range is confined to only $\ell \rightleftharpoons (\ell \pm 1)$ transitions. For the ion–dipole interaction,

$$V(\mathbf{r}, \mathbf{R}) = -\left(\frac{Ze^2}{R^2}\right) r\cos\theta \tag{4}$$

the exact time development operator has been obtained [1–5] in both classical and quantal formulations. The exact probabilities $P^{(n)}_{\ell'\ell}$ for the whole array of $\ell \to \ell'$ transitions were then extracted. The exact solutions were made possible by the inherent Group Dynamic Symmetry of the Rydberg atom together with the assumption of the ion–dipole interaction. A universal classical probability was deduced which allowed illustration of rapid convergence of the quantal to the classical results with increasing principal quan-

* Corresponding author.

1387-3806/$ – see front matter © 2008 Elsevier B.V. All rights reserved.
doi:10.1016/j.ijms.2008.08.017

tum number n. The structure exhibited in the variation of $P^{(n)}_{\ell'\ell}$ with ℓ' was explained and the Quantal–Classical Correspondence was displayed [1,2].

Exact solution is, however, not possible when higher-order multipole interactions are included. When the ion-quadrupole term which induces tree-like $\ell \rightleftharpoons \ell \pm 2$ transitions and higher terms are included in the expansion (3), then only numerical solutions are possible. Rather than adding the higher -order interactions one-by-one within some complicated theoretical formulation, we shall, in this paper, determine the probabilities $P^{(n)}_{\ell'\ell}$ for the Stark mixing process (1) from molecular dynamics simulations using the full ion–atom electrostatic interaction (2). In so doing, we shall be able to determine if and where higher multipoles are important to Stark mixing for the ultracold collision energies, of interest. If unimportant, then the exact analytical treatment [1,2] based on the ion–dipole interaction will be valid over a wide range of ultracold energies. Also, accurate molecular dynamics simulations are of interest here because other competing effects of radiative decay, black-body radiation and inelastic $n - n'$ collisions, which will assume significance as the collision energy is increased, can be easily incorporated, without the need for implementation of complex and difficult theory.

2. Simulation methodology

The present study of collisional Stark mixing is based on the Classical Trajectory Monte Carlo (CTMC) method. We start with a distribution of Rydberg atoms in a microcanonical ensemble with a given energy and angular momentum represented by the 'quantum numbers' n and ℓ. The orbital radius and velocity are $a_n = n^2 a_0$ and $v_n = v_0/n$, respectively, where a_0 and v_0 are the atomic units of length and velocity. The collision is confined to the $(Y - Z)$ plane of a Cartesian coordinate system. For each atom in the ensemble the initial position of the projectile is taken as $\mathbf{R}(X, Y, Z) = (0, b, z_0)$ in cartesian coordinates, where the impact parameter $Y = b$ is sampled from a distribution uniform in b^2, and where $z_0 = -vt_0$ is determined from the simulation time $2t_0$. With this distribution, we propagate each and every atom under a particular slowly varying potential due to the slowly passing ion at a given impact parameter b and relative collision-velocity v. The parameters here are the impact parameter b, relative velocity v, principal quantum number n, and the number $n_{\rm orb}$ of orbits of time period τ_n involved in the collision. The position vector from the target to the projectile is $\mathbf{R}(X, Y, Z) = (0, b, vt)$, where the time t runs in the interval from $-t_0 = -\tau_n n_{\rm orb}/2$ to $t_0 = \tau_n n_{\rm orb}/2$. The distribution over the final angular momentum ℓ' of the target Rydberg atoms after the collision is taken and analyzed. We adopt the Symplectic solver described in Ref. [7], because it is custom-made for these long time-scale simulations. In this way, the probabilities $P^{(n)}_{\ell'\ell}$ for $n\ell \rightarrow n\ell'$ transitions as a function of impact-parameter b can be extracted.

2.1. Stark mixing under the ion–dipole interaction

In order to test the accuracy of the molecular dynamics method, we first conduct simulations for the probabilities $P^{(n)}_{\ell'\ell}$ under the pure ion–dipole interaction (4) and then compare the results with the exact classical analytical probabilities, previously obtained [1,2]. Once high accuracy is established, the full interaction (2) will then be used. A convenient parameter for this simulation is the dimensionless Stark parameter, defined as the ratio of the Stark to collision frequencies and given by [1,2]

$$\alpha = \frac{3Z}{2\tilde{b}\tilde{v}} \tag{5}$$

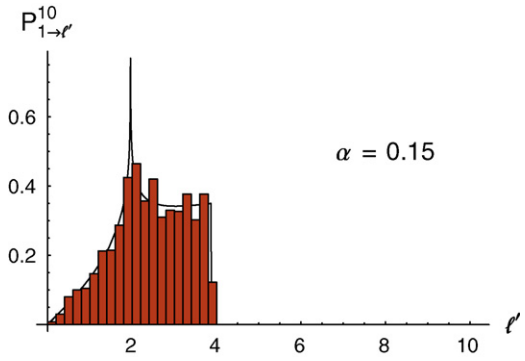

Fig. 1. Plot of Stark transition probabilities $P^{n}_{\ell\to\ell'}$ as a function of ℓ' for values of $\alpha = 3Z/2\tilde{b}\tilde{v} = 0.15$. Histograms are present simulations with $n_{\rm orb} = 100$ and curves are from analytical formula [1,2].

where $\tilde{v} = v/v_n$ and $\tilde{b} = b/a_n$ are the collision velocities and impact-parameters, scaled to the corresponding Rydberg units. The region $\alpha \leq 1$ of interest is the Orbital adiabatic and Stark sudden region, as explained in Ref. [1].

Some representative graphs comparing the results of the simulation with the exact theoretical probabilities are presented in Figs. 1 and 2.

The curves are given by the exact classical formula, Eq. (27) of Ref. [2] and the histograms are the present simulations with $n_{\rm orb} = 100$ for a sample of 2000 atoms. The agreement is excellent. This procedure will therefore be valuable for the study of Stark collisions under the full interaction (2), in the presence of black-body radiation or other competing processes, as electronic excitation/de-excitation/ionization which will become important as the collision-energy is increased. More refinement can be obtained by taking a larger sample of atoms, though at the cost of greater computational time. Cross-sections for Stark mixing can be obtained, if required, from

$$\sigma^{(n)}_{\ell'\ell}(v) = 2\pi \int_0^\infty P^{(n)}_{\ell'\ell}\, b\, {\rm d}b = \pi a_n^2 \left(\frac{9Z^2}{2\tilde{v}^2}\right) \int_0^\infty P^{(n)}_{\ell'\ell}(\alpha)\ \alpha^{-3}\, {\rm d}\alpha \tag{6}$$

under the provisor that the limit $b \to 0$ requires special consideration [1].

3. Dependence on simulation time and number of atoms

(A) The first factor that we analyze is the dependence of the final results on the number of orbits $n_{\rm orb}$ involved in the simulation. We test this case with a simulation for collision durations of

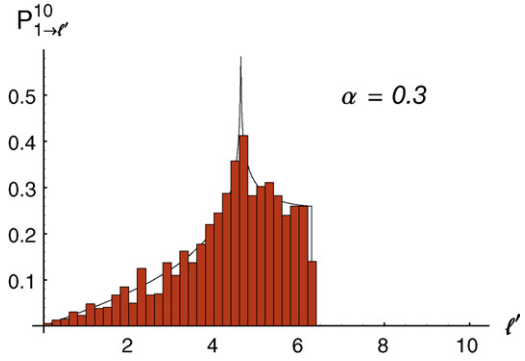

Fig. 2. Plot of Stark transition probabilities $P^{n}_{\ell\to\ell'}$ as a function of ℓ' for values of $\alpha = 3Z/2\tilde{b}\tilde{v} = 0.3$. Histograms are present simulations $n_{\rm orb} = 100$ and curves are from analytical formula [1,2].

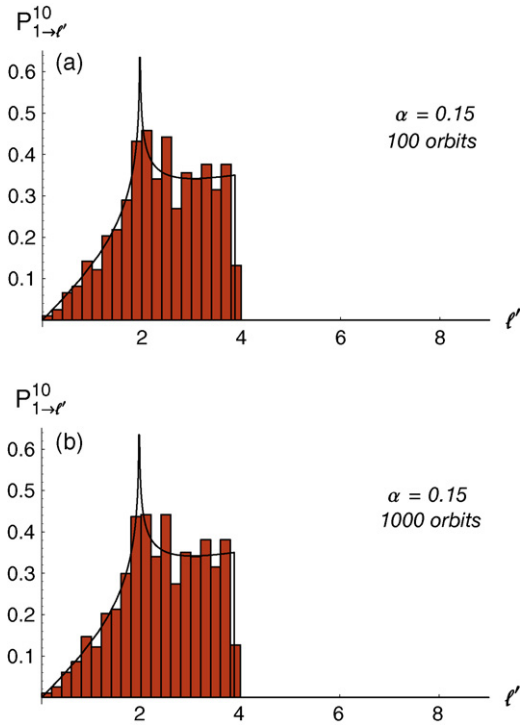

Fig. 3. Plot of Stark transition probabilities $P^n_{\ell\to\ell'}$ as a function of ℓ' for values of $\alpha = 3Z/2\tilde{b}\tilde{v} = 0.15$. Histograms are present simulations for (a) 100 orbits, (b) 1000 orbits and curves are from analytical formula [1,2].

100 orbits and 1000 orbits, with a sample of 1000 atoms. At the end of the simulation, atoms with fractional energy change less than 0.001 were retained, and then analyzed. The results for these two cases were identical and are displayed in Fig. 3(a) and (b) for $\alpha = 0.15$. For both the cases the integrator was set to take 800 time-steps per orbit. Because increasing the number of orbits or the simulation time did not affect the probabilities for a reasonable choice of α, the simulations are now restricted to 100 orbits.

(B) The sensitivity to the results of changing the number of atoms in the sample is now examined. We run this test for a (high) value of $\alpha = 0.6$. Fig. 4(a) and (b) correspond to 3000 and 1000 atoms, respectively. The previous classical spikes were removed by using the discretized probability density, defined via the trapezoidal rule as $P^n_{\ell\to\ell'} = (P^n_{\ell\to\ell'} + P^n_{\ell\to\ell'+\epsilon})/2$ with ϵ small, to be compared with the histograms from the simulation. For 3000 atoms, agreement with theoretical results becomes much better. Thus, increasing the number of atoms in the sample gives better accuracy, and 3000 atoms is therefore a reasonable number for this problem.

Here we have shown that the CTMC method is indeed a valuable computational approach for accurate classical probabilities, and can be a viable tool to investigate Stark mixing under the exact ion–atom (molecule) potential, and other perturbations.

4. Stark mixing under the full interaction

So far, we have made a dipole approximation (4) for the interaction between the projectile and the target. However, for higher

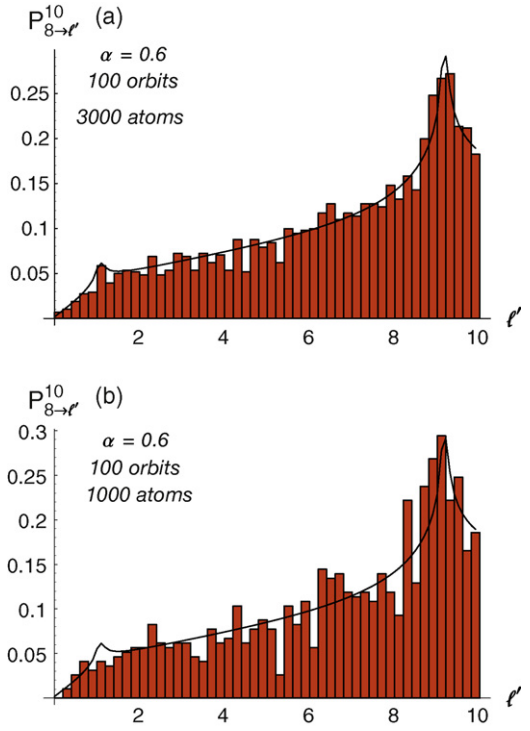

Fig. 4. Plot of Stark transition probabilities $P^n_{\ell\to\ell'}$ as a function of ℓ' for values of $\alpha = 3Z/2\tilde{b}\tilde{v} = 0.6$. Histograms are present simulations for (a) 100 orbits for 3000 atoms, (b) 100 orbits and 1000 atoms and curves are from analytical formula [1,2].

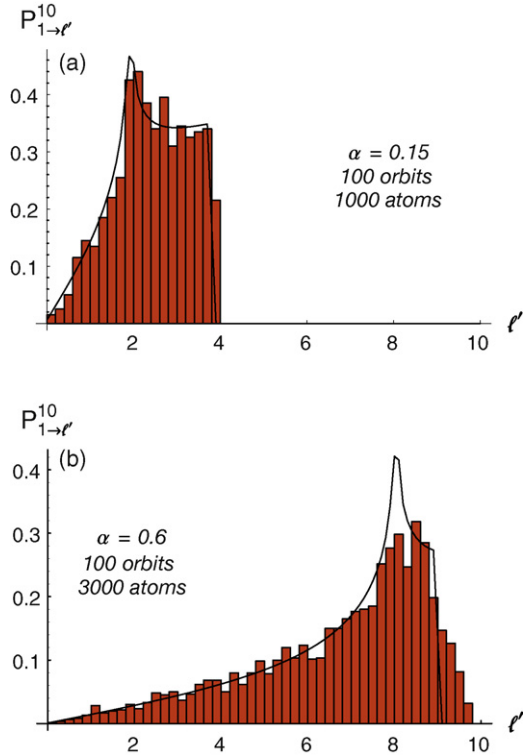

Fig. 5. (a) Plot of Stark transition probabilities $P^n_{\ell\to\ell'}$ as a function of ℓ' for values of $\alpha = 0.15$. Histograms from the simulation for 100 orbits with full interaction for 1000 atoms and curves from analytical results using the dipole interaction. (b) Plot of Stark transition probabilities $P^n_{\ell\to\ell'}$ as a function of ℓ' for values of $\alpha = 0.6$. Histograms are present simulations for 100 orbits with full interaction for 3000 atoms and curves are from analytical formula [1,2].

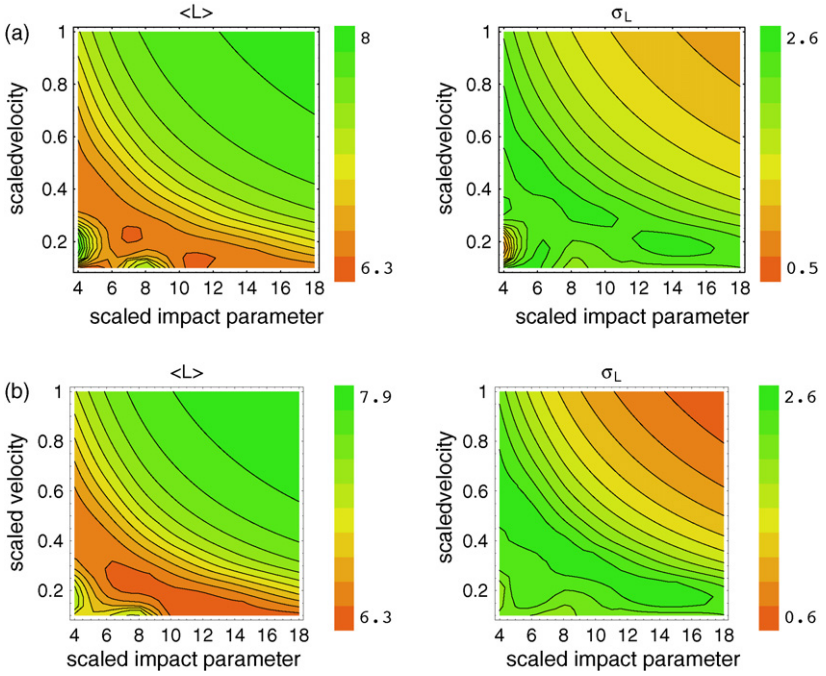

Fig. 6. Contour plots of $\langle L \rangle$ and σ_L as a function of scaled impact parameter and scaled velocity for the (a) ion–dipole and (b) full interaction for transitions from $\ell = 8$ and $n = 10$. Simulation uses 2000 atoms and 100 orbits and the above plot was interpolated using 80 points in the grid.

values of α (with smaller impact parameters b), this approximation could, in principle, break down. This effect can be investigated by using the exact electrostatic interaction (2) in the code and then observe how the higher multipoles affect the transition probabilities. Two representative cases are considered: (1) 1000 atoms, 100 orbits for $\alpha = 0.15$; (2) 3000 atoms, 100 orbits for $\alpha = 0.6$.

Fig. 5(a) shows the simulation for $\alpha = 0.15$ under the full interaction potential (2) between the projectile and the target. Here the probabilities are compared with the discretized probabilities for the dipole interaction. The two probabilities are in close agreement, which indicates that the quadrupole terms do not contribute and the dipole interaction is indeed valid at small α.

Fig. 5(b) shows the simulation under the full interaction potential (2) and $\alpha = 0.6$. The resulting probabilities are compared with the discrete analytical dipole probabilities. The code was run for 3000 atoms, which provides reasonable convergence (cf. Fig. 4) for $\alpha = 0.6$. It is noted that the probabilities from our simulation spill over to higher ℓ' values previously inaccessible for the pure dipole case. This is a clear indication of the importance of higher multipoles at higher values of α.

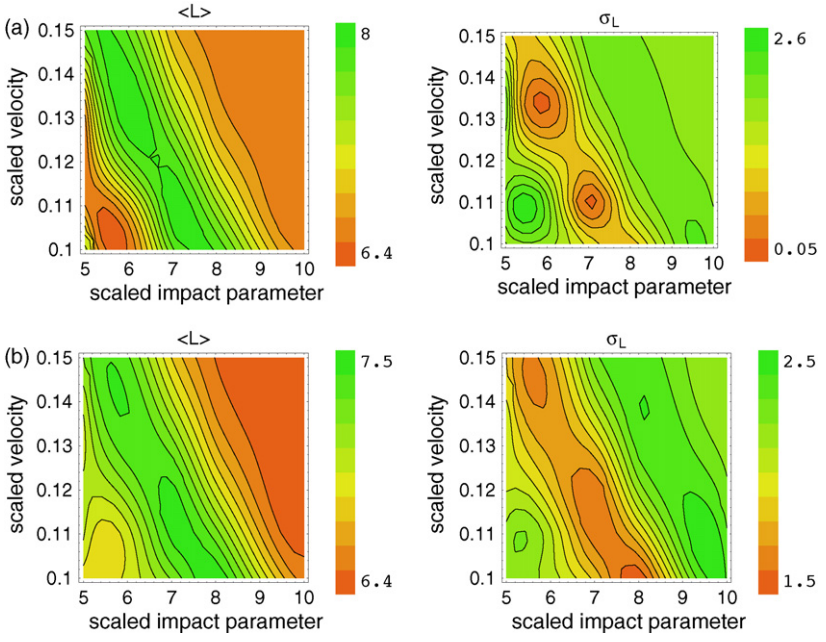

Fig. 7. Contour plots of $\langle L \rangle$ and σ_L as a function of scaled impact parameter and scaled velocity for the (a) ion- dipole and (b) full interaction for transitions from $\ell = 8$ and $n = 10$. Simulation uses 3000 atoms and 150 orbits and 66 point interpolation to render this plot.

4.1. Contour plots

In order to provide a qualitative picture of the collision-induced transitions in the ensemble and to illustrate the difference between the full interaction and dipole interaction, we examine contour plots of the mean $\langle L\rangle$ and standard deviation σ_L in the distribution over angular momentum L. The mean provides the location of the average peak of the distribution, and the standard deviation indicates the width of the distribution about the mean. Contour plots for $\langle L\rangle$ and σ_L, are shown in scaled impact parameter $\tilde{b} = b/a_n$ and scaled velocity $\tilde{v} = v/v_n$ space. Fig. 6(a) is for the ion–dipole interaction and Fig. 6(b) is for the full interaction. The $\langle L\rangle$-plots over the (4–18)-range in $\tilde{b}$ show very clearly where Stark mixing primarily occurs and provides quantitative justification of the qualitative Fig. 3 of Ref. [1], which illustrates the partitioning of the $(\tilde{b}, \tilde{v})$- region into different segments where various processes can occur.

Fig. 6(a) shows that the range of ℓ' widens for smaller $\tilde{b}$ and $\tilde{v}$ where α is larger, as is evident also from Fig. 5(a) and (b). This is because large α imply shorter collision times so that the distribution over final ℓ' is narrow, while the longer collision times associated with smaller α produce a broader distribution over final ℓ'. This is confirmed by the larger σ_L in Fig. 6(a). The full interaction produces a wider range in ℓ' which is reflected in Fig. 6(b). Stark mixing occurs mainly in the Orbital Adiabatic-Stark Sudden region [1], which is the green area of Fig. 6(a) and (b). The lower portions of Fig. 6(a) and (b) are now amplified in high-resolution contour plots (Fig. 7(a) and (b)) focus on low impact parameters, the (5–10)-range in $\tilde{b}$ and low collision velocities $\tilde{v}$. The green area in Fig. 7(a) for $\langle L\rangle$, i.e., where $\langle L\rangle \simeq 8$ and $\sigma_L \simeq 0$, represents the theoretical demarcation curve between the Stark sudden and Stark adiabatic regions where $\tilde{b} = 3Z/2\tilde{v}$ (cf., Fig. 3 of Ref. [1]). When the full interaction is adopted, then Fig.7(b) shows that angular momentum changes do occur in that region, evident also where $\sigma_L \simeq 1.5$.

5. Conclusion

In this paper, we have shown that Classical Trajectory Monte Carlo simulations, customized for long time-scales, are accurate and do reproduce the Stark mixing probabilities provided by the exact classical analytical solutions based on the ion–dipole interaction alone. The sensitivity of transition probabilities to various parameters – the initial distance of the projectile and the number of atoms used in the simulation – was examined. The dependence on the initial projectile distance z_0 was rather weak, while more atoms were required to get close agreement, particularly for higher values of α. Once the accuracy was established, the validity of using only the ion–dipole projectile–target interaction rather than the full interaction was then examined. We demonstrated that the dipole approximation is indeed valid for low values of $\alpha \sim 0.1$ while, at smaller impact-parameters higher multipoles do influence the overall final-state ℓ'- distribution at the larger ℓ', inaccessible to ion–dipole collisions alone. Contour plots illustrate the region of $\tilde{b}, \tilde{v}$-space important to Stark mixing and confirms the theoretical partitioning previously presented [1]. When the full interaction is used, the transition between the Stark adiabatic and Stark sudden regions become less pronounced than that for the pure dipole interaction.

This investigation has also provided a viable and feasible approach wherein effects (e.g., quantum defects, black-body radiation) and other competing processes (n-changing collisions, radiative cascade, etc.) can now be readily incorporated into a comprehensive treatment of ultracold Rydberg plasmas.

Acknowledgments

This research has been supported by AFOSR Grant No. FA95500-06-1-0212 and NSF Grant No. 04-00438. It is our pleasure to congratulate Professor Zdenek Herman on this occasion of his 75th birthday.

References

[1] D. Vrinceanu, M.R. Flannery, Phys. Rev. A 63 (2001) 032701.
[2] M.R. Flannery, D. Vrinceanu, Int. J. Mass. Spectrom. Ion Processes 223/224 (2003) 473.
[3] D. Vrinceanu, M.R. Flannery, Phys. Rev. Lett. 85 (2000) 4880.
[4] D. Vrinceanu, M.R. Flannery, J. Phys. B 33 (2000) L721.
[5] D. Vrinceanu, M.R. Flannery, J. Phys. B 34 (2001) L1.
[6] M.R. Flannery, D. Vrinceanu, in: Dissociative Recombination: Theory, Experiment, and Applications, Kluwer Academic/Plenum Press, Singapore, 2002.
[7] G.S. Balaraman, D. Vrinceanu, Phys. Lett. A 369 (2007) 188.